



Double-folding potentials from chiral effective field theory

V. Durant ^{a,b,*}, P. Capel ^{a,b,c}, L. Huth ^{a,b}, A.B. Balantekin ^d, A. Schwenk ^{a,b,e}



^a Institut für Kernphysik, Technische Universität Darmstadt, 64289 Darmstadt, Germany

^b ExtreMe Matter Institute EMMI, GSI Helmholtzzentrum für Schwerionenforschung GmbH, 64291 Darmstadt, Germany

^c Physique Nucléaire et Physique Quantique (CP 229), Université libre de Bruxelles (ULB), B-1050 Brussels, Belgium

^d Department of Physics, University of Wisconsin, Madison, WI 53706, USA

^e Max-Planck-Institut für Kernphysik, Saupfercheckweg 1, 69117 Heidelberg, Germany

ARTICLE INFO

Article history:

Received 14 August 2017

Received in revised form 18 May 2018

Accepted 30 May 2018

Available online 13 June 2018

Editor: W. Haxton

ABSTRACT

The determination of nucleus–nucleus potentials is important not only to describe the properties of the colliding system, but also to extract nuclear-structure information and for modelling nuclear reactions for astrophysics. We present the first determination of double-folding potentials based on chiral effective field theory at leading, next-to-leading, and next-to-next-to-leading order. To this end, we construct new soft local chiral effective field theory interactions. We benchmark this approach in the ^{16}O – ^{16}O system, and present results for cross sections computed for elastic scattering up to 700 MeV in energy, as well as for the astrophysical S -factor of the fusion reaction.

© 2018 The Author(s). Published by Elsevier B.V. This is an open access article under the CC BY license (<http://creativecommons.org/licenses/by/4.0/>). Funded by SCOAP³.

1. Introduction

Determining the interaction between two nuclei is a long-standing and challenging problem [1]. It constitutes an important input in the modelling of nuclear reactions, which provide key information about the structure of nuclei and are relevant for processes that take place in stars. The interaction between two nuclei has been modelled by phenomenological potentials, e.g., of Woods–Saxon form, whose parameters are adjusted to reproduce elastic-scattering data. Numerical potentials have also been obtained from inversion of scattering data [2]. Albeit precise when experimental data exist, these potentials lack predictive behavior and do not have controlled uncertainties. Alternatively, it has been suggested to construct nucleus–nucleus potentials from the densities of the colliding nuclei and a given nucleon–nucleon (NN) interaction using a double-folding procedure [3]. It is known that this framework provides more realistic potentials for the nucleon–nucleus interactions than for the nucleus–nucleus case [4]. Nevertheless, it constitutes a first-order approximation to optical potentials derived from Feshbach's reaction theory [1]. Interesting results have been obtained in such a way, e.g., by considering zero-range

contact NN interactions [5,6] or using a G -matrix approach, see, e.g., Refs. [7,8] for recent work.

During the last decade, there have been great advances in nuclear structure and nuclear reactions based on effective field theories (EFT). For example, chiral EFT has become the standard method for developing systematic nuclear forces rooted in the symmetries of quantum chromodynamics (see, e.g., Refs. [9–11] for recent reviews). Efforts have been made to derive nucleon–nucleus optical potentials using chiral EFT interactions from many-body perturbation theory [12,13] and self-consistent Green's function calculations [14,15]. In this work, we focus on the derivation of nucleus–nucleus potentials from chiral NN interactions and nucleonic densities. In particular, we use local chiral EFT interactions [16–22], because this simplifies the double-folding calculation.

In this first study, we explore and test this idea for ^{16}O – ^{16}O reactions, comparing our calculations to elastic-scattering [23–30] and fusion data [31–35]. For this system, phenomenological Woods–Saxon potentials [30] and potentials obtained through inversion techniques [36,37] also exist. We show that the double-folding potential and the reaction observables exhibit an order-by-order behavior expected in EFT and observe that, for soft potentials, our calculations have only a weak dependence on the regularization scale. The comparison of our results with experiment leads us to suggest various directions for improvements for constructing nucleus–nucleus potentials from chiral EFT interactions with the double-folding method.

* Corresponding author.

E-mail addresses: durant@theorie.ikp.physik.tu-darmstadt.de (V. Durant), pierre.capel@ulb.ac.be (P. Capel), lukashuth@theorie.ikp.physik.tu-darmstadt.de (L. Huth), baha@physics.wisc.edu (A.B. Balantekin), schwenk@physik.tu-darmstadt.de (A. Schwenk).

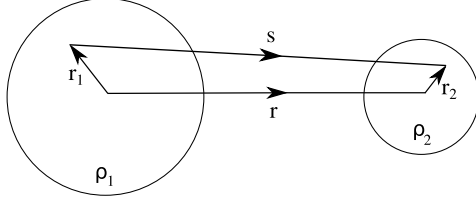


Fig. 1. Coordinates of the nuclei involved in the double-folding calculation.

This paper is organized as follows. We start with a brief review of the formalism for the double-folding potential in the following section. In Sec. 3, we discuss local chiral EFT interactions and the construction of new soft local chiral NN potentials. We then determine the double-folding potentials at different chiral orders and apply these to ^{16}O - ^{16}O elastic scattering in Sec. 4 and to the S -factor for $^{16}\text{O} + ^{16}\text{O}$ fusion in Sec. 5. Finally, we summarize and give an outlook in Sec. 6.

2. Double-folding potential: formalism

We consider the potential between nucleus 1 (with atomic and mass numbers Z_1 and A_1) and nucleus 2 (with Z_2 and A_2). In the double-folding formalism, the nuclear part of the nucleus-nucleus potential $V_F = V_D + V_{\text{Ex}}$ can be constructed from a given NN interaction v by double folding over the densities in the direct (D) channel and the density matrices in the exchange (Ex) channel. The review of the formalism for the double-folding potential in this section follows Ref. [7]. We will include only NN interactions here and leave the investigation of many-body contributions to future work.

In the direct channel, the double-folding potential is calculated by integrating the NN interaction over the neutron (n) and proton (p) density distributions $\rho_1^{n,p}$ and $\rho_2^{n,p}$ of the colliding nuclei,

$$V_D(\mathbf{r}) = \sum_{i,j=n,p} \iint \rho_1^i(\mathbf{r}_1) v_D^{ij}(\mathbf{s}) \rho_2^j(\mathbf{r}_2) d^3\mathbf{r}_1 d^3\mathbf{r}_2, \quad (1)$$

where \mathbf{r} is the relative coordinate between the center of mass of the nuclei, \mathbf{r}_1 and \mathbf{r}_2 are the coordinates from the center of mass of each nucleus, $\mathbf{s} = \mathbf{r} - \mathbf{r}_1 + \mathbf{r}_2$ (the geometry is shown in Fig. 1), and the sum i, j is over neutrons and protons with their respective densities.

To account for the antisymmetrization between nucleons, the double-folding potential receives contributions also from the exchange channel,

$$V_{\text{Ex}}(\mathbf{r}, E_{\text{cm}}) = \sum_{i,j=n,p} \iint \rho_1^i(\mathbf{r}_1, \mathbf{r}_1 + \mathbf{s}) v_{\text{Ex}}^{ij}(\mathbf{s}) \times \rho_2^j(\mathbf{r}_2, \mathbf{r}_2 - \mathbf{s}) \exp\left[\frac{i\mathbf{k}(\mathbf{r}) \cdot \mathbf{s}}{\mu/m_N}\right] d^3\mathbf{r}_1 d^3\mathbf{r}_2, \quad (2)$$

where $\mu = m_N A_1 A_2 / (A_1 + A_2)$ is the reduced mass of the colliding nuclei (with m_N the nucleon mass) and the integral is over the density matrices $\rho^i(\mathbf{r}, \mathbf{r} \pm \mathbf{s})$ of the nuclei. In the exchange channel, there is an additional phase that renders the double-folding potential dependent on the energy E_{cm} in the center-of-mass system. The momentum for the nucleus-nucleus relative motion \mathbf{k} is related to E_{cm} , the nuclear part of the double-folding potential, and the double-folding Coulomb potential V_{Coul} through

$$k^2(\mathbf{r}) = 2\mu \left[E_{\text{cm}} - V_F(\mathbf{r}, E_{\text{cm}}) - V_{\text{Coul}}(\mathbf{r}) \right]. \quad (3)$$

As a result, V_{Ex} has to be determined self-consistently. Note that at our level of calculation the double-folding potential, $V_F = V_D +$

V_{Ex} , is real. The density matrices entering in Eq. (2) are approximated using the density matrix expansion [38] restricted to its leading term,

$$\rho^i(\mathbf{r}, \mathbf{r} \pm \mathbf{s}) = \frac{3}{s k_F^i(\mathbf{R})} j_1(s k_F^i(\mathbf{R})) \rho^i(\mathbf{R}), \quad (4)$$

where $\mathbf{R} = \mathbf{r} \pm \mathbf{s}/2$, j_1 is a spherical Bessel function of the first kind, and we take the effective local Fermi momentum, which is an arbitrary scale in the density-matrix expansion, as in Ref. [7]:

$$k_F^i = \left[(3\pi^2 \rho^i)^{2/3} + \frac{5(\nabla \rho^i)^2}{12(\rho^i)^2} + \frac{5\nabla^2 \rho^i}{36\rho^i} \right]^{1/2}. \quad (5)$$

In the case of spherical nuclei, the densities and the effective local Fermi momenta depend only on the distance from the center of mass of the nucleus (r_i or R).

For doubly closed-shell nuclei, the NN interaction entering the double-folding potential in the direct and exchange channels, v_D and v_{Ex} , respectively, at this level receive contributions only from the central parts of nuclear forces. Then also the NN interaction and the double-folding potentials depend only on the relative distance (s or r). Writing the NN interaction in terms of their two-body spin-isospin components, v^{ST} , and distinguishing between proton-proton (pp), proton-neutron (pn, np), and neutron-neutron (nn) interactions, v_D and v_{Ex} read

$$v_{D,\text{Ex}}^{pp,nn}(s) = \frac{1}{4} [v^{01}(s) \pm 3v^{11}(s)], \quad (6)$$

$$v_{D,\text{Ex}}^{pn,np}(s) = \frac{1}{8} [\pm v^{00}(s) + v^{01}(s) + 3v^{10}(s) \pm 3v^{11}(s)], \quad (7)$$

where the upper (lower) signs refer to the direct (exchange) term and we have neglected the small isospin-symmetry-breaking corrections to v .

The densities of the colliding nuclei are an important input for the calculation of the double-folding potential. In this first study based on chiral EFT interactions, we adopt the two-parameter Fermi distributions provided by the São Paulo group [5] for the proton and neutron densities, whose parameters were fitted to Dirac–Hartree–Bogoliubov calculations

$$\rho^{p,n}(r) = \frac{\rho_0}{1 + \exp\left(\frac{r - R_{p,n}}{a_{p,n}}\right)}, \quad (8)$$

where $\rho_0 = 0.091 \text{ fm}^{-3}$ and the radii $R_{p,n}$ and diffusenesses $a_{p,n}$ depend on the proton and neutron numbers of the nucleus. Expressed in fm, they are given by

$$R_p = 1.81 Z^{1/3} - 1.12, \quad a_p = 0.47 - 0.00083 Z, \quad (9)$$

$$R_n = 1.49 N^{1/3} - 0.79, \quad a_n = 0.47 + 0.00046 N. \quad (10)$$

3. Local chiral EFT interactions

3.1. Nucleon–nucleon potentials

Chiral EFT provides a systematic expansion for nuclear forces using nucleons and pions as degrees of freedom, which is connected to the underlying theory of quantum chromodynamics [9, 10]. The different contributions to NN and many-nucleon interactions are ordered according to a power counting scheme in powers of $(Q/\Lambda_b)^\nu$, where Q is a typical momentum or the pion mass and Λ_b the breakdown scale of the theory of the order of 500 MeV. This leads to a hierarchy of two- and many-nucleon interactions, with NN interactions starting at leading order (LO, $\nu = 0$) followed

by a contribution at next-to-leading order (NLO, $\nu = 2$), whereas three-nucleon interactions enter at next-to-next-to leading order ($N^2\text{LO}$, $\nu = 3$).

Because they facilitate the calculation of double-folding potentials, we use local chiral NN interactions, developed initially in Refs. [16,17], but construct new soft NN interactions up to $N^2\text{LO}$. As in these references, the long- and short-range parts of the interaction are regularized by

$$f_{\text{long}}(r) = 1 - e^{-(r/R_0)^4} \quad \text{and} \quad f_{\text{short}}(r) = \frac{e^{-(r/R_0)^4}}{\pi \Gamma(3/4) R_0^3}, \quad (11)$$

where R_0 is the coordinate-space cutoff in the NN potentials used. The long-range regulator is designed to remove the singularity at $r = 0$ in the pion exchanges, while it preserves its properties at large distances. The short-range regulator smears out the NN contact interactions. A second cutoff Λ is used in the spectral-function regularization of the two-pion exchange, which enters first at NLO. In Refs. [16,17] it was shown that the calculations are practically insensitive to Λ for local interactions; in the present work, we consider $\Lambda = 1000$ MeV.

As it turns out, the available local interactions from Refs. [16,17] with $R_0 = 1.0$ fm and 1.1 fm are too hard (see also Ref. [40]) and, thus, not suitable for calculations of a nucleus–nucleus potential at the simple “Hartree–Fock” level¹ considered here, because the resulting double-folding potentials are repulsive. Additional NN attraction coming from beyond Hartree–Fock many-body contributions would solve this behavior of the resulting double-folding potentials. To perform calculations at the Hartree–Fock level, we can only use the existing interaction with $R_0 = 1.2$ fm. In order to estimate the impact of the regulator, we construct softer interactions with cutoffs $R_0 = 1.4$ fm and 1.6 fm. We determine the low-energy constants (LECs) by fitting to the np phase shifts from the Nijmegen partial wave analysis (PWA) [39]. To this end, we minimize the following χ^2

$$\chi^2 = \sum_i \frac{(\delta_i^{\text{PWA}} - \delta_i^{\text{theo}})^2}{\Delta \delta_i^2}, \quad (12)$$

computed from the squared difference between the PWA phase shifts and the calculated ones. The uncertainty $\Delta \delta_i^2$ is obtained from the PWA, a model uncertainty, and a numerical error:

$$\Delta \delta_i^2 = (\Delta \delta_i^{\text{PWA}})^2 + (\Delta \delta_i^{\text{mod}})^2 + (\Delta \delta_i^{\text{num}})^2. \quad (13)$$

For the model uncertainty we use a relative uncertainty multiplied with a constant value [22,41],

$$\Delta \delta_i^{\text{model, LO}} = \left(\frac{Q}{\Lambda_b} \right)^2 C, \quad (14)$$

$$\Delta \delta_i^{\text{model, } \nu} = \left(\frac{Q}{\Lambda_b} \right)^{\nu+1} C, \quad (15)$$

where $Q = \max(m_\pi, p = \sqrt{E_i^{\text{lab}} m_N/2})$ and $C = 1^\circ$. For both cutoffs ($R_0 = 1.4$ fm and 1.6 fm), we take $\Lambda_b = 400$ MeV, which also roughly corresponds to a coordinate-space cutoff $R_0 = 1.4$ fm to get a more conservative uncertainty estimate.

Our interactions are fit up to laboratory energies of 50 MeV at LO and up to 150 MeV at NLO and $N^2\text{LO}$. In particular, we consider

Table 1

Low-energy constants (LECs) for the soft cutoffs $R_0 = 1.4$ fm and 1.6 fm at LO, NLO and $N^2\text{LO}$. In the last row, the deuteron binding energy E_d , not used to constrain the LECs, is given in MeV; its experimental value is $E_d = 2.224$ MeV. The LO LECs C_S and C_T are given in fm^2 , the others are in fm^4 .

R_0 [fm]	1.4 fm			1.6 fm		
	LO	NLO	$N^2\text{LO}$	LO	NLO	$N^2\text{LO}$
C_S	-2.675	-0.480	1.331	-3.590	-0.988	0.538
C_T	-0.021	0.723	0.363	-0.188	0.660	0.495
C_1	0.124		-0.104		-0.098	-0.206
C_2	0.302	0.188		0.393	0.368	
C_3		-0.224	-0.217		-0.311	-0.278
C_4	0.192	0.166		0.312	0.267	
C_5		-2.268	-2.083		-2.416	-2.282
C_6	0.471	0.355		0.603	0.536	
C_7		-0.578	-0.529		-0.798	-0.790
E_d	1.886	2.151	2.193	2.043	2.147	2.178

the energies 1, 5, 10, 25, 50, 100, and 150 MeV. The LO interaction is fit to the two S -wave channels, while the NLO and $N^2\text{LO}$ interactions are also constrained by the four P -waves and the ${}^3S_1 - {}^3D_1$ mixing angle ε_1 . The LECs and the deuteron binding energy obtained for each interaction are given in Table 1. All other inputs and conventions for these softer local chiral NN potentials are as in Refs. [16,17]. The phase shifts for $R_0 = 1.4$ fm are shown in Fig. 2; we find similar results with $R_0 = 1.6$ fm. The phase shift reproduction here is comparable to the interactions from Refs. [16, 17].

3.2. Double-folding potential

To apply the double-folding method using local chiral NN interactions, we consider the ${}^{16}\text{O}-{}^{16}\text{O}$ system, where there are ample sets of data to which we can compare our calculations. Elastic scattering has been accurately measured at various energies [23–30] and these data sets have been precisely analyzed with phenomenological optical potentials [30,42] or using inversion techniques [36, 37]. This enables us to compare our results with state-of-the-art phenomenological calculations. At lower energy, the fusion of two ${}^{16}\text{O}$ nuclei [31–35] is another observable with which we can test our double-folding potential. In this section, we present results for the double-folding potential computed at different energies and we illustrate its order-by-order behavior and the sensitivity to the cutoff scale.

Fig. 3 shows the direct (upper panel) and exchange (lower panel) contributions to the double-folding potential based on the local chiral $N^2\text{LO}$ potential with $R_0 = 1.4$ fm. Since the NN interaction is energy independent, the direct contribution of the double-folding potential is also energy independent [see Eq. (1)]. The exchange contribution given by Eq. (2), however, includes an energy dependence through the relative momentum \mathbf{k} in the exponential factor [see Eq. (3)]. The shape of this exchange contribution does not vary significantly with energy, but its attractive strength decreases with increasing energy, which can be understood by the increasing variation of the exponential factor.

The final double-folding potential computed at different orders and with different cutoffs is displayed for $E_{\text{lab}} = 350$ MeV in Fig. 4. The order-by-order behavior is similar to what is observed in Fig. 2. As explained before, lower cutoffs ($R_0 < 1.2$ fm) provide harder NN interactions, which lead to repulsive double-folding potentials at LO and NLO. These interactions require the additional attraction expected to come from many-body contributions beyond the simple Hartree–Fock level considered here. At $N^2\text{LO}$, the calculations have been performed with three different NN cutoffs: $R_0 = 1.2$ fm (dotted line), 1.4 fm (solid line), and 1.6 fm (dashed line); the lowest cutoff providing the less attractive potential. It is interesting to

¹ The double-folding potential is calculated at the Hartree–Fock level, but using phenomenological densities, which would otherwise be deficient, when taking them from a Hartree–Fock calculation based on NN interactions.

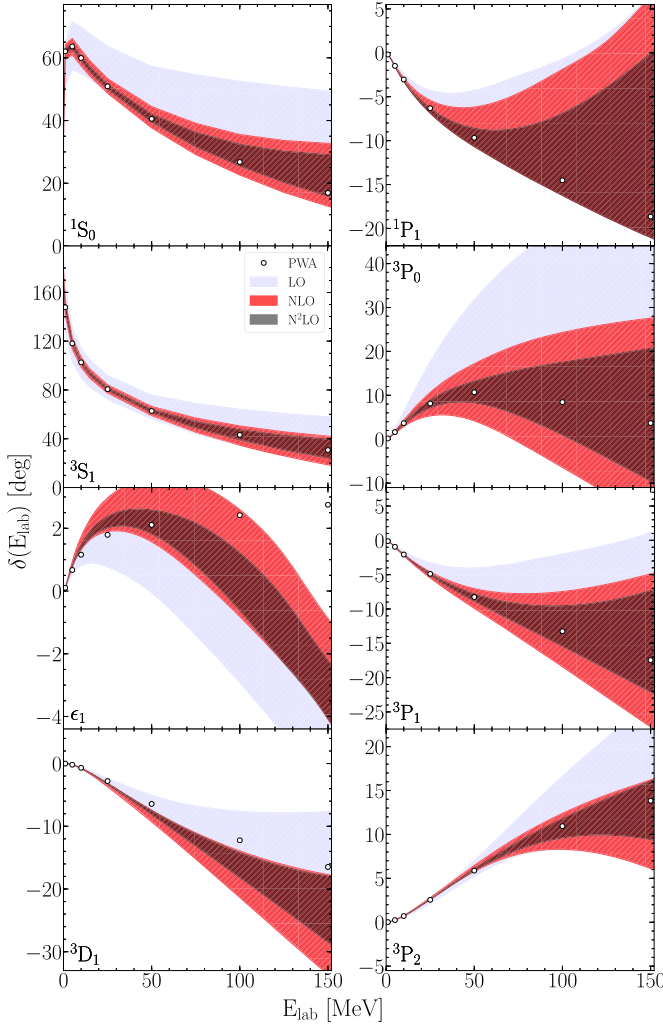


Fig. 2. Phase shifts for $R_0 = 1.4$ fm in different partial waves as a function of laboratory energy. Results are shown for the LO (blue), NLO (red), and N^2 LO (grey) interactions compared to the Nijmegen partial wave analysis (PWA) [39]. The bands at each order give the theoretical uncertainty as discussed in the text. (For interpretation of the colors in the figure(s), the reader is referred to the web version of this article.)

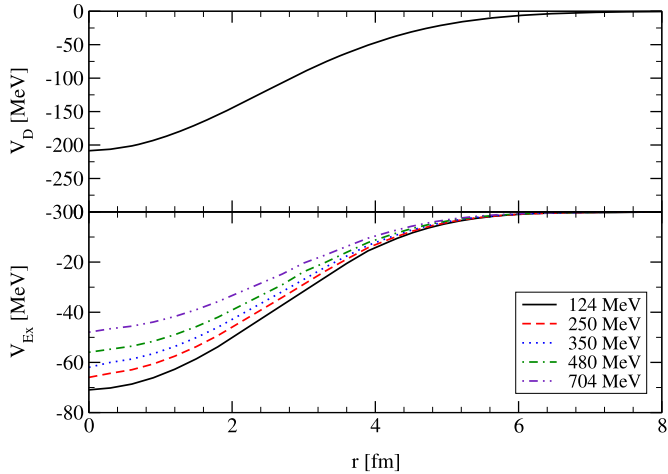


Fig. 3. Direct (upper panel) and exchange (lower panel) contributions to the double-folding potential for the ^{16}O - ^{16}O system based on the local chiral EFT interaction at $N^2\text{LO}$ with $R_0 = 1.4$ fm. The direct contribution is energy independent and we show results for different laboratory energies, E_{lab} , in the exchange channel.

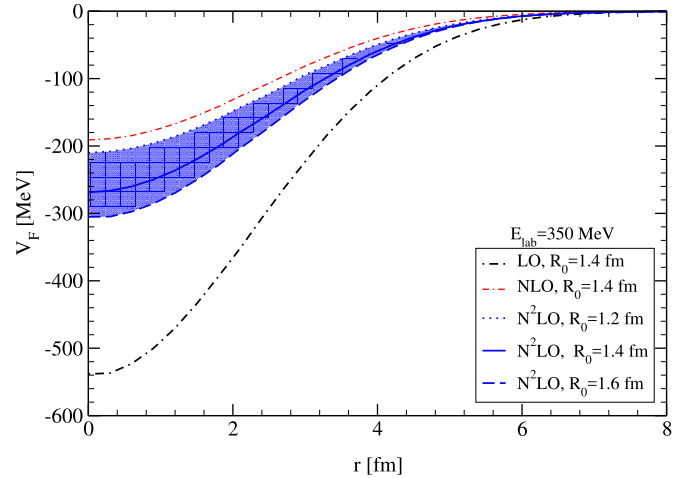


Fig. 4. Double-folding potential for the ^{16}O - ^{16}O system at $E_{\text{lab}} = 350$ MeV. The results obtained at LO, NLO, and $N^2\text{LO}$ (for $R_0 = 1.4$ fm) illustrate the order-by-order behavior, while the shaded area at $N^2\text{LO}$ shows the sensitivity to the cutoff for $R_0 = 1.2, 1.4$, and 1.6 fm.

notice that the sensitivity to the NN cutoff R_0 decreases at larger distance, where all three $N^2\text{LO}$ potentials present nearly identical asymptotics. The range of the regularization cutoff, R_0 , highlighted by the shaded band in Fig. 4, will allow us to gauge the level of details needed in NN interactions to reproduce the physical observables in nucleus-nucleus reactions.

4. Elastic scattering

The elastic scattering of medium to heavy nuclei can be described within the optical model. In that model, the nuclear part of the interaction between the colliding nuclei is described by a complex potential. Roughly speaking, the real part corresponds to the attractive interaction between the nuclei, whereas the imaginary part simulates the absorption of the incoming channel to other open channels, such as inelastic scattering or transfer. Double-folding potentials are often used for the real part of the optical potential. In this first study, we follow the São Paulo group and assume the imaginary part of the optical potential U_F to be proportional to its real part [6]

$$U_F(r, E_{\text{cm}}) = (1 + i N_W) V_F(r, E_{\text{cm}}), \quad (16)$$

where V_F is our double-folding potential and N_W is a real coefficient taken in the range 0.6–0.8.

The cross section for ^{16}O - ^{16}O elastic scattering for laboratory energy $E_{\text{lab}} = 350$ MeV is shown in Fig. 5 as a ratio to the Mott cross section. In these calculations, we take for the imaginary part $N_W = 0.8$, whereas we study the sensitivity to N_W later. Note that since ^{16}O is a spinless boson, the wave function for the ^{16}O - ^{16}O relative motion needs to be properly symmetrized.

As in Figs. 2 and 4, we observe a systematic order-by-order behavior. The uncertainty related to the cutoff choice at $N^2\text{LO}$ (shaded area) is similar to that observed in the double-folding potential itself (see Fig. 4). At forward angles, i.e., up to 10° , the agreement of our calculations with experiment is excellent, knowing in particular that there are no parameters fitted to reproduce the data. At larger angles this agreement deteriorates. Since the spread observed in the NN cutoff band remains small even at larger angles, this discrepancy cannot be fully explained by the detail of the NN interactions considered. It is likely due to the simple Hartree-Fock level of the many-body calculation or to the

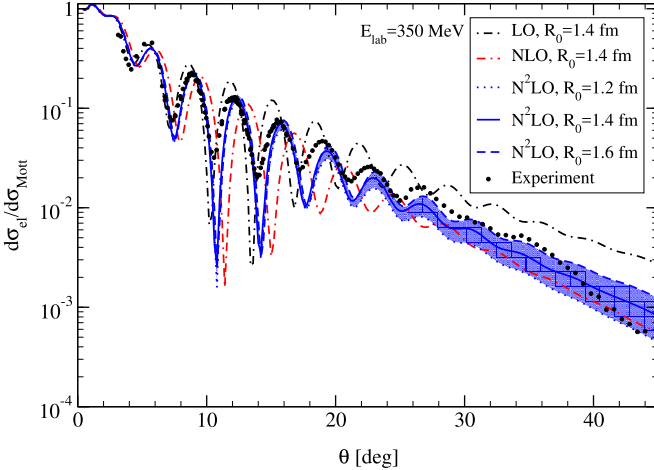


Fig. 5. Ratio of the cross section for elastic $^{16}\text{O}-^{16}\text{O}$ scattering to the Mott cross section for laboratory energy $E_{\text{lab}} = 350$ MeV. Results are shown at LO, NLO, and N^2LO for $R_0 = 1.4$ fm, and the sensitivity to $R_0 = 1.2-1.6$ fm is illustrated at N^2LO by the shaded area. In all cases, we take for the imaginary part $N_W = 0.8$ [see Eq. (16)]. The results are compared to experimental data from Ref. [24].

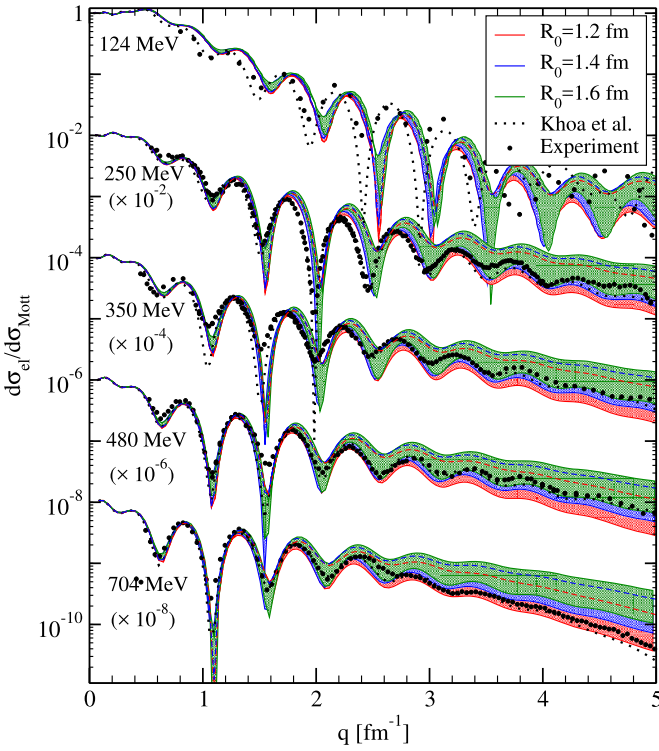


Fig. 6. Ratio of the cross section for elastic $^{16}\text{O}-^{16}\text{O}$ scattering to the Mott cross section as a function of momentum transfer q for various laboratory energies (the different energy results are offset by a factor as indicated). Results are shown at N^2LO for $R_0 = 1.2$ fm (red), 1.4 fm (blue), and 1.6 fm (green). For these cutoffs, the region between the results with $N_W = 0.6$ (upper limit) and $N_W = 0.8$ (lower limit) is shaded. In the case of $R_0 = 1.2$ fm and 1.4 fm, the upper line is shown as a dashed line. For comparison, we also show the optical-potential results of Khoa et al. [30] and the experimental data from Refs. [24,26–30]. (For interpretation of the colors in the figure(s), the reader is referred to the web version of this article.)

choice of the ^{16}O density, which could be improved. In addition, it could also reflect the simple description of the imaginary part. The elastic scattering cross sections computed at various laboratory energies between 124 and 704 MeV are displayed in Fig. 6 as a ratio to the Mott cross section. To compare the calculations

performed at different energies, we plot them as a function of the momentum transfer q . The bands are delimited by results for the range $N_W = 0.6-0.8$. Results generated by the cutoffs $R_0 = 1.2$ fm, 1.4 fm, and 1.6 fm are displayed in red, blue, and green, respectively. We find that the cutoff variation is less relevant than the impact of the imaginary part coefficient N_W . As in Fig. 5, we observe a general agreement between our calculations and the data, especially at forward angles. At larger momentum transfer, the agreement is less good, although the experimental points remain close to the spread obtained for the N_W range. This confirms that going beyond the simple description of the imaginary part could improve our calculations.

For comparison, we also show the cross sections computed with the phenomenological optical potential developed by Khoa et al. [30] (dotted line in Fig. 6). This potential, containing nine adjustable parameters that are modified at each energy, provides a near-perfect reproduction of the data. Given that we do not include any adjustable parameter to fit the data, our results with the double-folding potential based on chiral EFT interactions are therefore very encouraging.

5. Fusion reactions

The $^{16}\text{O} + ^{16}\text{O}$ fusion reaction is another test for our double-folding potential. This cross section σ_{fus} has been measured at low energies to study the role of intermediate resonances during fusion [31,32] and because this reaction takes place in medium- to heavy-mass stars [32–35]. Oxygen fusion is crucial in medium-mass nuclei burning chains, which provide the seeds to the synthesis of heavy elements. At low energy, the reaction takes place through quantum tunneling of the effective potential barrier that results from the combination of the attractive strong interaction, the repulsive Coulomb interaction, and the centrifugal term of the kinetic energy:

$$V_{\text{eff}}(r, E_{\text{cm}}) = V_F(r, E_{\text{cm}}) + V_{\text{Coul}}(r) + \frac{l(l+1)}{2\mu r^2}. \quad (17)$$

Since the fusion reaction takes place at very low energies and involves light spherical nuclei, we take the (real) double-folding potential as the nuclear interaction for this reaction [43]. For light systems like $^{16}\text{O} + ^{16}\text{O}$, the fusion barrier is at around 9 fm, well before the neck formation, which justifies the use of the double-folding procedure. For the code used in the computation of the fusion cross section, we approximate the Coulomb interaction by a sphere-sphere potential of radius $R_C = 2 \times 4.39$ fm [44]. We do not expect this change from the double-folding Coulomb term used in Eq. (3) to affect significantly our results.

The fusion cross section of $^{16}\text{O} + ^{16}\text{O}$ can be obtained from the probability P_l to tunnel through the barrier in each of the partial waves [43]

$$\sigma_{\text{fus}}(E_{\text{cm}}) = \frac{\pi}{k^2} \sum_l (1 + (-1)^l)(2l+1) P_l(E_{\text{cm}}). \quad (18)$$

The probabilities P_l are determined using the incoming-wave boundary condition detailed in Ref. [43] and implemented in the code CCFULL [45], in which we have included the effects of the symmetrization of the wave function for the fusing nuclei being identical spinless bosons.

At low energy, the fusion process is strongly hindered by the Coulomb repulsion. This effect is well accounted for by the Gamow factor, which is usually factorized out of the cross section to define the astrophysical S factor

$$S(E_{\text{cm}}) = E_{\text{cm}} e^{2\pi\eta} \sigma_{\text{fus}}(E_{\text{cm}}), \quad (19)$$

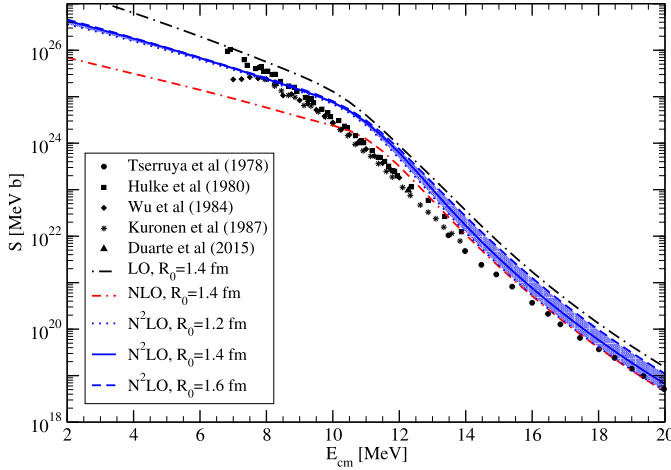


Fig. 7. Astrophysical S -factor for the fusion of $^{16}\text{O} + ^{16}\text{O}$ as a function of the energy E_{cm} in the center-of-mass system. Results are shown at LO, NLO, and N^2LO for $R_0 = 1.4 \text{ fm}$, and the sensitivity to $R_0 = 1.2\text{--}1.6 \text{ fm}$ at N^2LO is illustrated by the shaded area. The results are compared to experimental data from Refs. [31–35].

where the Sommerfeld parameter is given by $\eta = Z_1 Z_2 e^2 / (4\pi \varepsilon_0 v)$, with v the relative velocity between the two nuclei.

The S factor obtained at LO, NLO, and N^2LO for $R_0 = 1.4 \text{ fm}$ and with different cutoffs R_0 at N^2LO is displayed in Fig. 7. Given the very weak energy dependence of the double-folding potential observed at the relevant energies, V_{Ex} is taken at the center of the energy range, $E_{\text{cm}} = 12 \text{ MeV}$. We have tested that taking a different energy in this range leads to indistinguishable results from those in Fig. 7. It is interesting to note that, due to the nearly cutoff-independent asymptotic behavior of the nuclear folding potential, the spread between the results obtained with different values of R_0 is small around the Coulomb barrier. This leads to results at N^2LO in Fig. 7 that are closer than what Fig. 4 would suggest. Note also that the less attractive potentials (at NLO with $R_0 = 1.4 \text{ fm}$, and N^2LO with $R_0 = 1.2 \text{ fm}$) naturally lead to the lowest fusion cross sections. The general agreement with the data is good, recalling that there is no fitting parameter. As for elastic scattering, we observe that the sensitivity to the details in the NN interaction shown by the shaded area can only partially explain the discrepancy with experiment. In future work, we will explore how a better many-body calculation of the double-folding potential and more realistic densities of the fusing nuclei may improve this agreement.

6. Summary and outlook

We have presented a first study of constructing nucleus-nucleus potentials from local chiral NN interactions [16,17,22] using the double-folding method applied to the $^{16}\text{O}-^{16}\text{O}$ system. Our results show that for soft cutoffs, $R_0 \gtrsim 1.4 \text{ fm}$, the resulting double-folding potential exhibits a systematic order-by-order behavior expected in EFT and a weak cutoff dependence on the details of the NN interactions used. These features carry through to the elastic scattering cross section and the S -factor for the fusion reaction.

We have focused on the $^{16}\text{O}-^{16}\text{O}$ reactions, because these have been accurately measured and are well studied theoretically [23–35,42]. In all cases, a good agreement with the data has been obtained without any fitting parameter. Our results thus suggest that the idea to derive nucleus-nucleus potentials using the double-folding method based on local chiral EFT interactions is very promising.

We consider this a first step in a more fundamental description of nucleus-nucleus potentials, but there are several directions how the calculations can be improved, both at the level of the input interactions and the many-body folding method. First, the influence of the nucleon density of the colliding nuclei needs to be evaluated. This can be done by using more realistic densities, such as those obtained from electron-scattering measurements or accurate nuclear-structure models. Second, we need to refine the imaginary part of the potential. Assuming it to be proportional to the double-folding potential provides a first estimate, but it is clear that this can be improved. Comparisons with phenomenological potentials [30] and potentials built from inversion techniques [36, 37] can also provide tests towards more realistic prescriptions. In a calculation beyond Hartree-Fock, an imaginary part as well as non-local contributions would arise (see, e.g., Refs. [46,47]). Moreover, going beyond the level of the density-matrix expansion considered here, there will be gradient corrections [38] (i.e., surface terms) to the double-folding potential. Finally three-nucleon interactions need to be investigated in this approach, as they also enter at N^2LO .

In conclusion, coupling chiral EFT interactions with the double-folding method provides nucleus-nucleus potentials that lead to very encouraging agreement with elastic-scattering and fusion data in a broad range of energies. This idea is thus a promising first step towards the construction of microscopic optical potentials from first principles with control over uncertainty estimates. Through the above future developments, we hope to improve this new method to obtain a systematic way to build efficient optical potentials for nuclear reactions.

Acknowledgements

We thank J.E. Lynn and I. Tews for many helpful discussions, and in particular for providing the code for the local chiral interactions as well as for discussions on the softer local chiral interactions presented here. We also thank D. Baye for helpful discussions on the reactions studied in this work, and the International Atomic Energy Agency that provided the experimental data through their web page www-nds.iaea.org. This work was supported in part by the European Research Council Grant No. 307986 STRONGINT, the GSI-TU Darmstadt cooperation, the European Union's Horizon 2020 research and innovation programme under Grant Agreement No. 654002, and the US National Science Foundation Grant No. PHY-1514695.

References

- [1] M. Brandan, G. Satchler, Phys. Rep. 285 (1997) 143.
- [2] H. Leeb, H. Fiedeldey, R. Lipperheide, Phys. Rev. C 32 (1985) 1223.
- [3] G. Satchler, W. Love, Phys. Rep. 55 (1979) 183.
- [4] C. Mahaux, R. Sartor, Nucl. Phys. A 530 (1991) 303.
- [5] L.C. Chamon, B.V. Carlson, L.R. Gasques, D. Pereira, C. De Conti, M.A.G. Alvarez, M.S. Hussein, M.A. Candido Ribeiro, E.S. Rossi Jr., C.P. Silva, Phys. Rev. C 66 (2002) 014610.
- [6] D. Pereira, J. Lubian, J.R.B. Oliveira, D.P. de Sousa, L.C. Chamon, Phys. Lett. B 670 (2009) 330.
- [7] T. Furumoto, W. Horiuchi, M. Takashina, Y. Yamamoto, Y. Sakuragi, Phys. Rev. C 85 (2012) 044607.
- [8] K. Minomo, M. Kohno, K. Ogata, Phys. Rev. C 93 (2016) 014607.
- [9] E. Epelbaum, H.-W. Hammer, U.-G. Meißner, Rev. Mod. Phys. 81 (2009) 1773.
- [10] R. Machleidt, D.R. Entem, Phys. Rep. 503 (2011) 1.
- [11] H.-W. Hammer, A. Nogga, A. Schwenk, Rev. Mod. Phys. 85 (2013) 197.
- [12] J.W. Holt, N. Kaiser, G.A. Miller, W. Weise, Phys. Rev. C 88 (2013) 024614.
- [13] M. Vorabbi, P. Finelli, C. Giusti, Phys. Rev. C 93 (2016) 034619.
- [14] J. Rotureau, P. Danielewicz, G. Hagen, F.M. Nunes, T. Papenbrock, Phys. Rev. C 95 (2017) 024315.
- [15] A. Idini, C. Barbieri, P. Navrátil, Acta Phys. Pol. B 48 (2017) 273.
- [16] A. Gezerlis, I. Tews, E. Epelbaum, S. Gandolfi, K. Hebeler, A. Nogga, A. Schwenk, Phys. Rev. Lett. 111 (2013) 032501.

- [17] A. Gezerlis, I. Tews, E. Epelbaum, M. Freunek, S. Gandolfi, K. Hebeler, A. Nogga, A. Schwenk, Phys. Rev. C 90 (2014) 054323.
- [18] J.E. Lynn, J. Carlson, E. Epelbaum, S. Gandolfi, A. Gezerlis, A. Schwenk, Phys. Rev. Lett. 113 (2014) 192501.
- [19] I. Tews, S. Gandolfi, A. Gezerlis, A. Schwenk, Phys. Rev. C 93 (2016) 024305.
- [20] J.E. Lynn, I. Tews, J. Carlson, S. Gandolfi, A. Gezerlis, K.E. Schmidt, A. Schwenk, Phys. Rev. Lett. 116 (2016) 062501.
- [21] J.E. Lynn, I. Tews, J. Carlson, S. Gandolfi, A. Gezerlis, K.E. Schmidt, A. Schwenk, Phys. Rev. C 96 (2017) 054007.
- [22] L. Huth, I. Tews, J.E. Lynn, A. Schwenk, Phys. Rev. C 96 (2017) 054003.
- [23] E. Stiliaris, H. Bohlen, P. Fröbrich, B. Gebauer, D. Kolbert, W. von Oertzen, M. Wilpert, T. Wilpert, Phys. Lett. B 223 (1989) 291.
- [24] H.G. Bohlen, E. Stiliaris, B. Gebauer, W. von Oertzen, M. Wilpert, T. Wilpert, A. Ostrowski, D.T. Khoa, A.S. Demyanova, A.A. Ogloblin, Z. Phys. A 346 (1993) 189.
- [25] Y. Sugiyama, Y. Tomita, H. Ikezoe, Y. Yamanouchi, K. Ideno, S. Hamada, T. Sugimitsu, M. Hijiya, Y. Kondō, Phys. Lett. B 312 (1993) 35.
- [26] Y. Kondō, Y. Sugiyama, T. Tomita, Y. Yamanouchi, H. Ikezoe, K. Ideno, S. Hamada, T. Sugimitsu, M. Hijiya, H. Fujita, Phys. Lett. B 365 (1996) 17.
- [27] G. Bartnitzky, A. Blazevic, H.G. Bohlen, J.M. Casandjian, M. Chartier, H. Clement, B. Gebauer, A. Gillibert, T. Kirchner, D.T. Khoa, et al., Phys. Lett. B 365 (1996) 23.
- [28] F. Nuoffer, G. Bartnitzky, H. Clement, A. Blazevic, H.G. Bohlen, B. Gebauer, W. Von Oertzen, M. Wilpert, T. Wilpert, A. Lepine-Szily, et al., Nuovo Cimento A 111 (1998) 971.
- [29] M.P. Nicoli, F. Haas, R.M. Freeman, N. Aissaoui, C. Beck, A. Elanique, R. Nouicer, A. Morsad, S. Szilner, Z. Basrak, et al., Phys. Rev. C 60 (1999) 064608.
- [30] D.T. Khoa, W. von Oertzen, H.G. Bohlen, F. Nuoffer, Nucl. Phys. A 672 (2000) 387.
- [31] I. Tserruya, Y. Eisen, D. Pelte, A. Gavron, H. Oeschler, D. Berndt, H.L. Harney, Phys. Rev. C 18 (1978) 1688.
- [32] G. Hulke, C. Rolfs, H.P. Trautvetter, Z. Phys. A 297 (1980) 161.
- [33] S.-C. Wu, C. Barnes, Nucl. Phys. A 422 (1984) 373.
- [34] A. Kuronen, J. Keinonen, P. Tikkanen, Phys. Rev. C 35 (1987) 591.
- [35] J.G. Duarte, L.R. Gasques, J.R.B. Oliveira, V.A.B. Zagatto, L.C. Chamom, N. Medina, N. Added, W.A. Seale, J.A. Alcántara-Núñez, E.S. Rossi Jr., et al., J. Phys. G 42 (2015) 065102.
- [36] L. Allen, L. Berge, C. Steward, K. Amos, H. Fiedeldey, H. Leeb, R. Lipperheide, P. Fröbrich, Phys. Lett. B 298 (1993) 36.
- [37] M.T. Bennett, C. Steward, K. Amos, L.J. Allen, Phys. Rev. C 54 (1996) 822.
- [38] J.W. Negele, D. Vautherin, Phys. Rev. C 5 (1972) 1472.
- [39] V.G.J. Stoks, R.A.M. Klomp, M.C.M. Rentmeester, J.J. de Swart, Phys. Rev. C 48 (1993) 792.
- [40] J. Hoppe, C. Drischler, R.J. Furnstahl, K. Hebeler, A. Schwenk, Phys. Rev. C 96 (2017) 054002.
- [41] B.D. Carlsson, A. Ekström, C. Forsén, D.F. Strömborg, G.R. Jansen, O. Lilja, M. Lindby, B.A. Mattsson, K.A. Wendt, Phys. Rev. X 6 (2016) 011019.
- [42] Y. Kondō, F. Michel, G. Reidemeister, Phys. Lett. B 242 (1990) 340.
- [43] K. Hagino, N. Takigawa, Prog. Theor. Phys. 128 (2012) 1061.
- [44] D. Baye, N. Pecher, Nucl. Phys. A 379 (1982) 330.
- [45] K. Hagino, N. Rowley, A.T. Kruppa, Comput. Phys. Commun. 123 (1999) 143.
- [46] H. Feshbach, Ann. Phys. 5 (1958) 357.
- [47] H. Feshbach, Ann. Phys. 19 (1962) 287.